Lifetime measurements and shape coexistence in Sr97

Esmaylzadeh, A.; Régis, J.-M.; Kim, Y. H.; Köster, U.; Jolie, J.; Karayonchev, V.; Knafla, L.; Nomura, Kosuke; Robledo, L. M.; Rodríguez-Guzmán, R.

Source / Izvornik: **Physical Review C, 2019, 100**

Journal article, Published version
Rad u časopisu, Objavljena verzija rada (izdavačev PDF)

https://doi.org/10.1103/physrevc.100.064309

Permanent link / Trajna poveznica: https://urn.nsk.hr/urn:nbn:hr:217:802061

Lifetime measurements and shape coexistence in ^{97}Sr

A. Esmaylzadeh,[1,*] J.-M. Régis,[1] Y. H. Kim,[2] U. Köster,[2] J. Jolie,[1] V. Karayonchev,[1] L. Knafla,[1] K. Nomura,[3] L. M. Robledo,[4,5] and R. Rodríguez-Guzmán[6]

[1]*Universität zu Köln, Mathematisch-Naturwissenschaftliche Fakultät, Institut für Kernphysik, D-50937 Köln, Germany*
[2]*Institut Laue-Langevin, 71 Avenue des Martyrs, 38042 Grenoble, France*
[3]*Department of Physics, Faculty of Science, University of Zagreb, 10000 Zagreb, Croatia*
[4]*Departamento de Física Teórica, Universidad Autónoma de Madrid, E-28049 Madrid, Spain*
[5]*Center for Computational Simulation, Universidad Politécnica de Madrid, Campus de Montegancedo, Boadilla del Monte, E-28660 Madrid, Spain*
[6]*Physics Department, Kuwait University, 13060 Kuwait, Kuwait*

(Received 30 July 2019; revised manuscript received 2 September 2019; published 13 December 2019)

Delayed γ rays from neutron-rich $A = 97$ fission fragments were measured using the Lohengrin spectrometer at the high-flux reactor of the Institut Laue-Langevin in Grenoble. Several lifetimes of excited states in ^{97}Sr were measured using the fast-timing technique. The nucleus ^{97}Sr exhibits shape coexistence and is located exactly at the border of the spherical ($N \leqslant 58$) and deformed ($N \geqslant 60$) ground-state deformation. It is of particular interest to study the shape-coexisting structures at the spherical-deformed border ($N = 59$). The determined lifetimes within this work are compared to an interacting boson-fermion model calculation that is based on the microscopic energy density functional to provide a better understanding of the spherical-deformed border in strontium isotopes.

DOI: 10.1103/PhysRevC.100.064309

I. INTRODUCTION

Shape transitions in the A $\approx$ 100 region have been the subject of intense studies lately. The rapid change from the near spherical ^{96}Sr to the strongly deformed ^{98}Sr is well known [1,2]. Due to the proton subshell closures at $Z = 38$ ($\pi p_{3/2}$) and at $Z = 40$ ($\pi p_{1/2}$) and the neutron subshell closures at $N = 50$ ($\nu g_{9/2}$), $N = 56$ ($\nu d_{5/2}$), and $N = 58$ ($\nu s_{1/2}$), the $N =$ 50–58 ($^{88-96}$Sr) strontium and ($^{90-98}$Zr) zirconium isotopes have the low-energy structure of a semimagic nucleus. By increasing the number of neutrons crossing $N = 60$ a rapid change in ground-state deformation is observed, which results in a prolate-deformed ground-state rotational band in ^{98}Sr. This rapid change in shape occurs also for Zr ($Z = 40$) and is more smooth for lower Z, i.e., the Kr nuclei and, for higher Z, i.e., the Mo-Pd nuclei. In Sr, Y, and Zr nuclei with $N = 58$ and 59, low-lying spherical states coexist with deformed rotational bands that appear around 1 MeV [3–7]. Further there is experimental evidence in ^{98}Sr and ^{100}Zr for an additional prolate-oblate shape coexistence [8–10], which is underlined by theoretical calculations [11,12]. This variety of different structures and configurations causes the complexity of this region but also provides a lot of potential to understand the transition from single-particle to collective behavior.

To improve the understanding of such a rapid change, which can result in the phenomenon of shape coexistence, it is of particular interest to study the nuclei at the spherical-deformed border, in this case at $N = 59$. Shape coexistence has been proposed for ^{97}Sr in different works [5,6,13,14], where a spherical ground state and a rotational band structure have been assumed. The first two excited states possess a spherical shape, whereas above 550 keV few rotational bands start to evolve, i.e., on top of the $3/2^+$ state at 585.1 keV, the $(3/2)^-$ state at 644.7 keV, the $5/2^+$ state at 687.1 keV, the $(5/2)^-$ state at 713.8 keV, and the isomeric state $9/2^+$ at 830.8 keV. A possible description of the deformed states is given by the fact that once the neutron $\nu g_{7/2}$ orbit is being filled an interaction between $\nu g_{7/2}$ and $\pi g_{9/2}$ causes the proton subshell to vanish and results in a collective motion [15–17].

Another description, especially for the deformed states, is given by the Nilsson approach, which relies on the strong interaction between proton and neutron Nilsson orbitals [14]. The down-sloping $\nu 1/2^+[550]$ and $\nu 3/2^-[541]$ orbitals, which both result from the spherical $\nu h_{11/2}$ orbital, are the main forces that drive the deformation. The $\nu 9/2^+[404]$ orbital is a key factor in stabilizing the deformation at a saturation level of about $\beta \approx 0.4$, in which β represents the axially symmetric deformation [18]. The proton Nilsson orbitals $\pi g_{1/2}[440]$ and $\pi g_{3/2}[431]$ originating from the spherical $\pi g_{9/2}$ orbital are fully occupied for Sr with $Z = 38$ and Zr with $Z = 40$, respectively. The spatial overlap from the neutron orbitals with the proton orbitals creates a minimum in binding energy at a deformation level of 0.4, which at $N = 60$ is favored rather than the spherical configuration.

To study the phenomenon of shape coexistence and to assign the energy levels to the spherical or deformed

*Corresponding author: aesmaylzadeh@ikp.uni-koeln.de

configuration of the nucleus a fast-timing experiment at the Institut Laue-Langevin in Grenoble using the Lohengrin spectrometer was performed. The results should give a better understanding at the spherical-deformed border of the strontium isotopes. Especially, the $(3/2^+, 5/2^+)$ state at 522 keV is very important to understand where the rotational structure of the nucleus starts to be favored. In addition, with the newly gained knowledge a spin assumption about this state is made on the basis of the transitions and the level lifetime. The assignment of levels is underlined by calculations within the framework of the interacting boson approximation. A self-consistent mean-field calculation that is based on an energy density functional (EDF) is used to determine the parameter of the interacting boson-fermion model (IBFM) Hamiltonian.

This work is organized as follows. In Sec.II the experiment and the setup is explained in detail. Section III describes the fast-timing method that has been used to obtain the level lifetimes. In Sec. IV the analysis procedures for the measured lifetimes are presented. In Sec. V, the calculations and the discussion are explained and compared to the experimental results. In this section we especially discuss the state at 522 keV, where we give a suggestion for the spin and the parity according to the obtained results. Finally, a conclusion is given in Sec. VI.

II. EXPERIMENTAL DETAILS

Delayed γ rays from neutron-rich $A = 97$ fission fragments using the Lohengrin mass spectrometer were measured at the high-flux reactor of the Institut Laue-Langevin in Grenoble [19–21]. The nucleus of interest was produced and populated by a thermal-neutron-induced fission of a 0.7 cm $\times$ 7 cm $^{235}UO_2$ target with a thickness of 363 μg/cm^2. The fission yield for ^{97}Sr was about 1.7%. A 0.25-μm-thick Ni foil covered the target to reduce sputtering ^{235}U [22]. To investigate the mass $A = 97$ nuclei, especially ^{97}Sr, the Lohengrin spectrometer is able to select the fission products according to their mass- and energy-to-ionic-charge ratios with a vertical electric deflector and a horizontal magnetic deflector. The additional reverse energy dispersive (RED) magnet focused ions arriving in the focal plane to a beam spot that was collimated to 3 $\times$ 1 cm [19,20]. Further the fission products could be identified by their energy loss in a ΔE_1-ΔE_2 ionization chamber (hereafter called IC). The chamber was filled with isobutane (C_4H_{10}) at a pressure of 15 mbar. The target chamber contained an aluminum foil that was used as a stopper of the fission fragments. Four cylindrical 1.5″ $\times$ 1.5″ $LaBr_3$ (Ce) scintillator detectors (hereafter called LaBr) were installed with a relative angle of (90° to each of the neighboring detectors around the implantation zone. The compact detector ring was made such that the corners of detector heads were touching each other. They had a distance of about 2.2 cm to the center of the focal plane of the implantation zone. To minimize the distance and therefore maximize the efficiency of the setup no shielding of any kind was used. Furthermore, a typical lead shielding would introduce x-ray emissions in the energy region of interest for other experiments that were performed during the campaign, utilizing the same setup. For further details about timing effects in the low-energy region in particular on the effect of x-rays the reader is referred to Ref. [23]. In addition, two unshielded Clover detectors consisting of four germanium crystals each were used to monitor the γ rays, because the resolution of the LaBr was insufficient to resolve transitions that were close in energy. All Clover detectors were placed below the implantation zone. The measurement time was 1 week with a reduction in ion rates over the experiment dropping from 9000 to 3000 ions/s, due to target burnup.

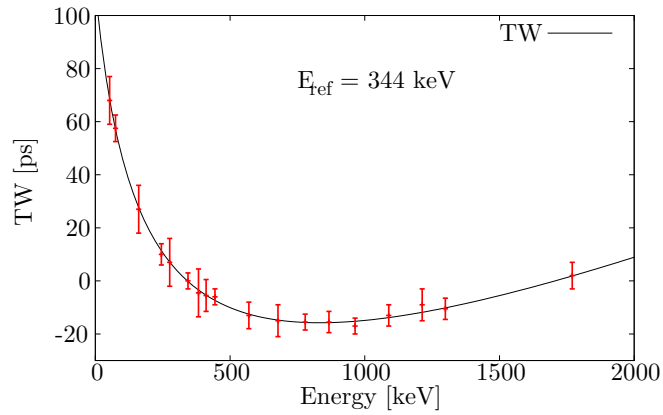

FIG. 1. The calibrated time-walk (TW) curve relative to the energy $E = 344$ keV. The standard deviation is calculated and the 2σ interval is chosen to be the error of the TW curve with 3 ps.

III. FAST-TIMING METHOD

To perform subnanosecond lifetime measurements at the Lohengrin spectrometer, the ionization chamber gated γ-γ fast-timing technique using LaBr detectors was employed. The ionization chamber gate ensures that the isomer of interest is selected, which leads to clean LaBr coincidence spectra with few γ rays and reduced Compton background. To measure lifetimes two LaBr detectors and an analog time-to-amplitude converter (TAC) were used to determine the time difference between two γ rays feeding and de-exciting an excited state of interest (see Refs. [24,25] for details). The time-stamped data were sorted offline to generate IC-LaBr-LaBr events for the lifetime determination. The events were used to construct a so-called symmetric energy-energy-time-difference cube, where the energy axis are symmetric under the exchange of E_1 and E_2, whereas the time-difference is antisymmetric under exchange [24,25].

A time alignment of the six detector-detector combinations was performed to improve the time resolution of the superimposed time-differences. The total γ-γ time differences were incremented twice, in two identical mirror-symmetric time-difference distributions, with mirror-symmetric mean time walk characteristics relative to a constant reference time t_0 [25], which is consistent with the generalized centroid difference method (described in Refs. [24,26]). To obtain the mean time-walk curve, which is energy dependent and shown in Fig. 1, full energy peaks (FEP) from the ^{152}Eu, ^{133}Ba, ^{207}Bi, ^{185}Os, and ^{187}W γ-ray sources have been used. The 2σ standard deviation is 3 ps and corresponds to the accuracy of the mean time walk. A detailed description of the

mean time-walk calibration procedure is given in Ref. [25]. Exact knowledge of the time walk is necessary to perform high-precision lifetime measurements using the well-known centroid shift method [27], where the centroid of a time distribution $D(t)$ is given by

$$C[D(t)] = \frac{\sum_{t_{\min}}^{t_{\max}} t\mathrm{D(t)}}{\sum_{t_{\min}}^{t_{\max}} D(t)}. \quad (1)$$

The centroid of the antisymmetric time-difference distributions can be written as [25]

$$C_{\mathrm{FEP}}(E_{\mathrm{feeder}}, E_{\mathrm{decay}}) = t_0 + \mathrm{TW}(E_{\mathrm{feeder}}, E_{\mathrm{decay}}) + \tau, \quad (2)$$

where τ is the mean lifetime of the excited state. To determine the lifetime the present fast-timing data are corrected for the time walk with $\mathrm{TW}(E_1, E_2) = \mathrm{TW}(E_1) - \mathrm{TW}(E_2)$ [25], where the values are derived from the curve in Fig. 1. The reference time is adjusted to $t_0 = 0$, so that the mean lifetime corresponds to the centroid $C_{\mathrm{FEP}}(E_1 = E_{\gamma_{\mathrm{feeder}}}, E_2 = E_{\gamma_{\mathrm{decay}}}) - \mathrm{TW}(E_1 = E_{\gamma_{\mathrm{feeder}}}, E_2 = E_{\gamma_{\mathrm{decay}}})$. As the subscript "FEP" indicates, this only holds for events where no time-correlated background is present. An analytical background time correction is used to interpolate the time-correlated background at the energy of interest, which has been shown to be most reliable [2,28–30]:

$$C_{\mathrm{FEP}} = C_{\mathrm{exp}} + \overline{t_{\mathrm{cor}}}, \quad (3)$$

with the average of both background contributions stemming from both peaks corresponding to the transition of interest. This leads to

$$\overline{t_{\mathrm{cor}}} = \tfrac{1}{2}[t_{\mathrm{cor}}(E_{\mathrm{decay}}) + t_{\mathrm{cor}}(E_{\mathrm{feeder}})], \quad (4)$$

where

$$t_{\mathrm{cor}}(E_{\mathrm{feeder(decay)}}) = \frac{C_{\mathrm{exp}} - C_{\mathrm{BG}}}{p/b_{\mathrm{feeder(decay)}}}. \quad (5)$$

C_{exp} is the experimentally determined centroid of the FEP, p/b is the peak-to-background ratio, and C_{BG} is the centroid of the background at the considered γ-ray energy. The background time response at the position of the FEP cannot be measured directly. To determine C_{BG} an interpolation is used where the measurement of centroids from several background time spectra around the FEP is necessary. With the obtained data points from background time spectra the centroid C_{BG} at the FEP can be interpolated and the formulas (3)–(5) can be used to get the centroid of the FEP (C_{FEP}). The uncertainty is calculated via the Gaussian error propagation.

IV. ANALYSIS

In this section the measured lifetimes are presented. In Fig. 2 the level scheme of ^{97}Sr and the full spectrum of the LaBr and Clover detectors after applying a gate on the IC chamber are presented. In Fig. 2 the transitions below the isomer are observed, which are in agreement with previous experiments [31]. The disturbing lines that are next to the lines of interest are removed by gating on any transition of ^{97}Sr. Most of the contamination transitions belong to the daughter nuclei of ^{97}Sr, i.e., ^{97}Y, ^{97}Zr, and ^{97}Nb. Some of

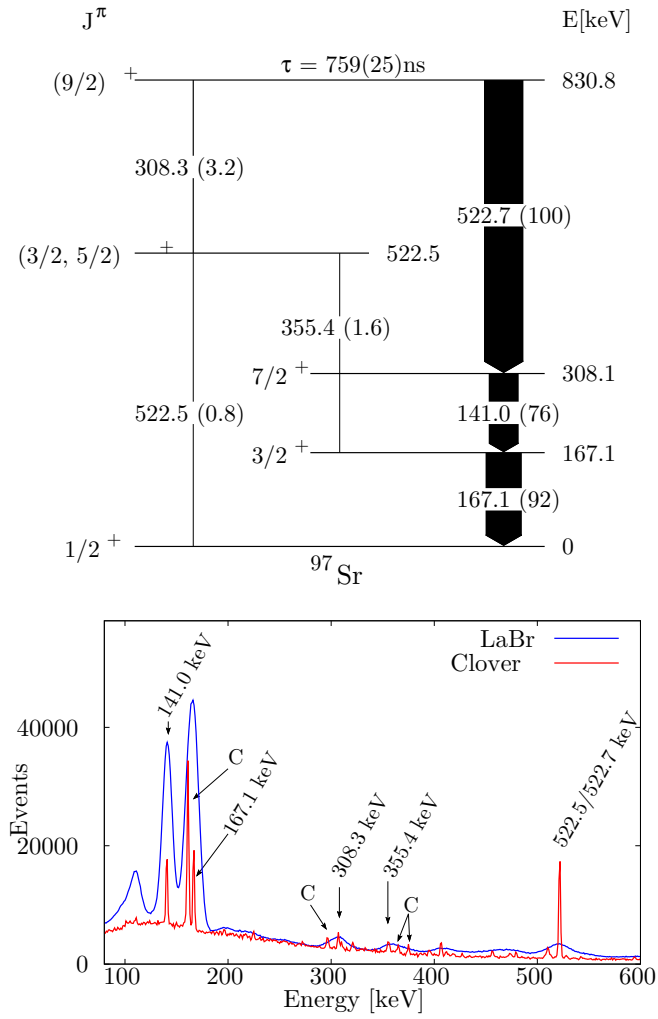

FIG. 2. Upper panel: The level scheme of ^{97}Sr below the isomeric $(9/2)^+$ state at 830.8 keV. Within the brackets the relative intensities of the transitions are given. The scheme only contains transitions observed in this work. In a similar experiment a $(3/2, 5/2)^+ \rightarrow 7/2^+$ (214.4 keV) transition has been observed [31] which is included in the calculation for the transition probabilities. Lower panel: Mass $A = 97$ gated coincidence spectra using the ionization chamber of the Lohengrin setup. The important lines of ^{97}Sr and the contaminates are indicated.

the contaminants belong to ^{88}Br, which has nearly the same mass over charge ratio as ^{97}Sr.

All lifetimes are measured using a gate on the ionization chamber and two LaBr gates that act as start and stop signals, respectively. The Clover detectors are used to monitor the measured γ rays and to assure that no contamination is lying close to the peaks, which cannot be fully resolved by the insufficient energy resolution of the LaBr detectors. In a first step the IC gate is combined with a LaBr gate to obtain doubly gated Clover spectra and check for disturbing transitions. After being sure that the transition of interest is free of any contamination, the IC-LaBr-LaBr gates are used to generate time distributions. The lifetimes are then obtained via the method explained in Sec. III. The final results are summarized in Table II.

A. Lifetime of the $3/2^+$ state

The $3/2^+$ state is located at 167.1 keV and is the first excited state of ^{97}Sr. After applying a 3-μs gate on the ionization chamber the decay transition (167.1 keV) shows a contaminant with an energy of 161.2 keV that is the $7/2^+_1 \rightarrow 3/2^+_1$ transition in ^{97}Zr, which disappears after using LaBr coincidence gates. To measure the lifetime of the $3/2^+$ one can select the strong feeder-decay cascade of 141.0–167.1 keV by applying a gate on the feeder or decay transition. The results of the applied gates are shown in Figs. 3(f) and 3(g), where Clover and LaBr spectra with an IC gate and a LaBr gate on 167.1 and 141.0 keV, respectively, were applied. As highlighted in the figure both transitions are clearly visible without any contaminants. Further the peak-to-background ratio (p/b) is around 20, which leads to a nearly background-free time spectrum as pictured in Fig. 3(h). To determine the lifetime three different methods were used, i.e., the convolution method, the slope method, and the centroid-shift method. All three results are consistent within the errors in which the determined lifetime from the centroid-shift method (explained in Sec. III) with $\tau_{3/2^+} = 448(4)$ ps is adopted. In the literature the lifetime of the state is reported to 317(57) ps [32] and 1.5 ns [33], where neither can be confirmed. The authors of Ref. [32] used planar high-purity germanium detectors, which have a time resolution worse than that of the LaBr detectors used in this work. Furthermore, the time response of the detector system is not mentioned, which could lead to the assumption that this has not been investigated. Reference [33] just mentions the 1.5-ns lifetime, but does not explain how and with which method the lifetime has been measured. Due the missing explanation of the references and the improved lifetime measurement technique in the present work, the newly determined lifetime appears more reliable.

B. Lifetime of the $(3/2, 5/2)^+$ state

To determine the lifetime of the $5/2^+$ state at 522.5 keV the $(9/2)^+ \rightarrow (5/2)^+ \rightarrow 3/2^+$ (308.3–355.4 keV) cascade and the $(9/2)^+ \rightarrow (5/2)^+ \rightarrow 1/2^+$ (308.3–522.5 keV) cascade are used. A gate on mass $A = 97$ and a LaBr gate on 355.4(308.3) keV were applied as shown in Figs. 3(a) and 3(b). As explained in Sec. III an interpolation of the background time response was performed to correct for the background time response that can disturb the time distribution of the feeder-decay cascade [see Figs. 3(c) and 3(d)]. The two resulting time distributions, which are generated with $E_{\mathrm{ref}} = 308.3(355.4)$ keV lead to the final centroid shift of 8(6) ps. After performing the interpolation of the background time response and using Eqs. (3)–(5) the final lifetime results in 14(8) ps for the 308.3–355.4 keV cascade and 15(10) ps for the 308.3–522.5 keV cascade and thus a weighted average of $\tau_{(3/5,5/2)^+} = 14(6)$ ps is obtained.

C. Lifetime of the isomeric $7/2^+$ and $9/2^+$ states

To measure the lifetimes of the isomeric states, we used the time stamps of the detectors. A combination of all three detectors ensures that the transitions are free from contamination and other disturbing effects. For both lifetimes a gate on the ionization chamber was applied. To generate a time distribution for the $7/2^+$ state a LaBr gate on the 522.7-keV transition and a Clover gate on the decaying 141.0-keV transition were used. The fast LaBr detector was used as a trigger while the slower germanium Clover detector was used for the lifetime measurement. The Clover gate was used as the stop signal and the time-stamp difference was generated and shows the decay of the $7/2^+$ state. The same gates were applied for the $9/2^+$ state, but with the trigger enabled for the ionization chamber, which then acted as the start signal and the LaBr detector acted as the stop signal. To improve the background noise level and to be sure that it was free of contamination the Clover gate was also applied. The lifetime of the $7/2^+$ state with $\tau_{7/2^+} = 252(10)$ ns agrees with the results of previous experiments, which are 245(14) ns [33], 238(6) ns [34], and 238(36) ns [35]. The literature for the $9/2^+$ state provides contradictory results. On the one hand the lifetime values are 382(39) ns [36] and 368(43) ns [35]. Another result is 551(16) ns [37], where it does not seem certain that the measured 522.4-keV γ ray is from ^{97}Sr [37]. The last group of results are on the order of 750 ns, like 759(19) ns [38], 750^{+231}_{-173} ns [39], and 743(14) ns [31], in which the measured lifetime of the present work, 759(25) ns, also falls.

V. CALCULATIONS AND DISCUSSION

In this section the results from this work are discussed and compared to theoretical calculations. For this purpose calculations using the Interacting Boson-Fermion model (IBFM) [40] based on the microscopic energy density functional (EDF) are used. Microscopic calculation for odd-mass nuclei is generally quite complicated because both the collective and the single-particle degrees of freedom have to be treated on the same footing. In the theoretical framework employed in the present study, the interacting boson model (IBM) Hamiltonian for the even-even core nucleus (^{96}Sr) is completely determined from a microscopic EDF calculation, and also the key ingredients of the single-fermion and fermion-boson coupling Hamiltonians, i.e., single-particle energies and occupation probabilities, are provided by the fully microscopic calculation. Even at the cost of having to fit a few strength parameters for the boson-fermion interaction terms so as to reproduce with reasonable accuracy experimental data for excitation spectra in each odd-mass nucleus, this semimicroscopic IBFM calculation provides a detailed description of spectroscopy in odd-mass systems in a computationally very efficient way. After giving a short description of the IBFM model that has been used, the energy levels from the calculation and the experiment are compared to each other. Further, transition strengths, which were calculated from the lifetime, are discussed. Also, a suggestion of the spin and the parity for the $(3/2, 5/2)^+$ state at 522 keV is given based on the lifetime measurement and the IBFM calculation.

A. Theoretical framework

Note that only a superficial description with the important formulas and features of the model is given. For a more detailed description the reader is referred to Refs. [41–44].

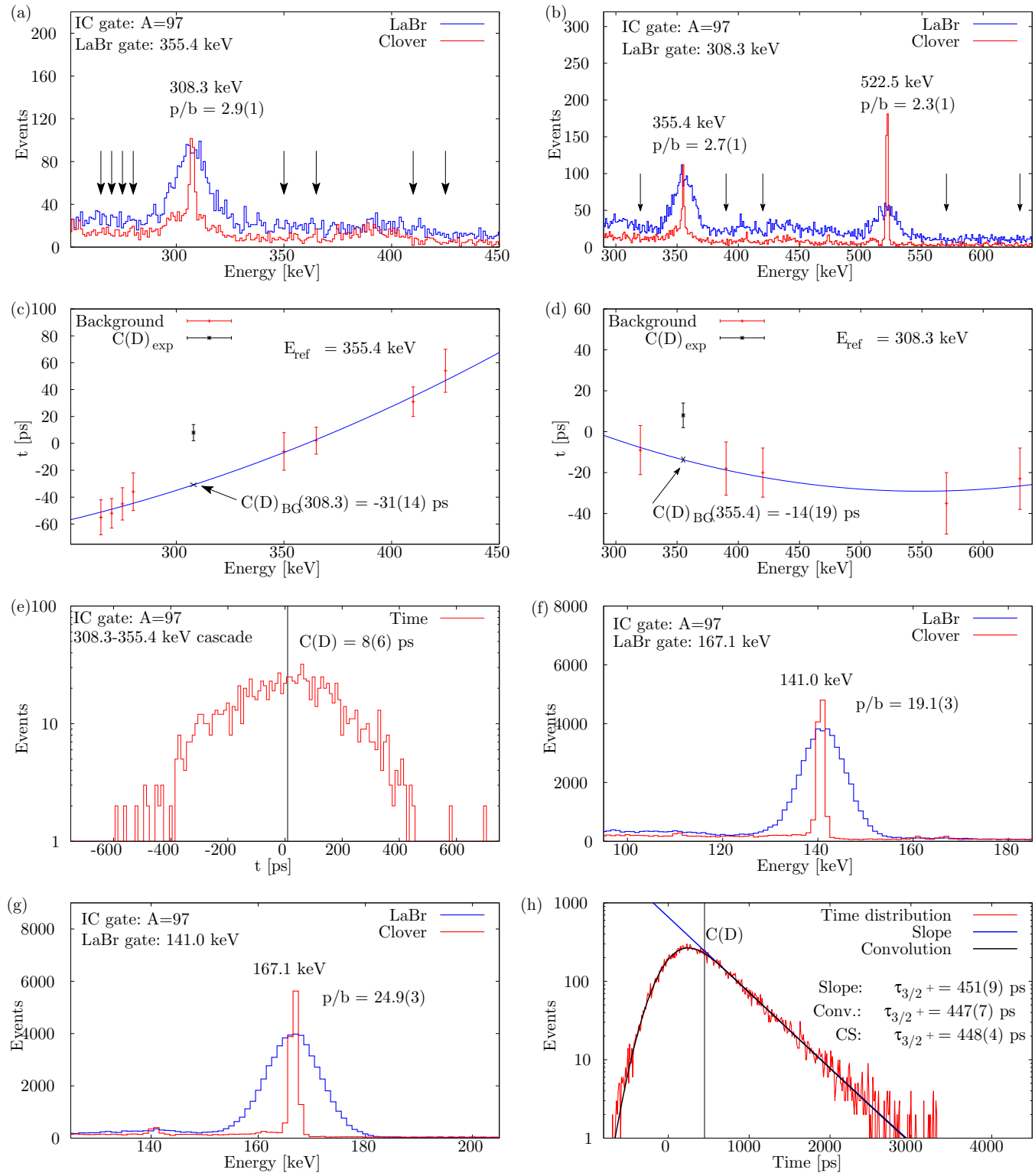

FIG. 3. (a) The 308.3-keV transition after applying a 3-μs gate on $A = 97$ on the ionization chamber and a LaBr gate on the $(3/2, 5/2)^+ \rightarrow 3/2^+$ (355.4 keV) transition. (b) The 355.4- and the 522.5-keV transition after applying a 3-μs gate on $A = 97$ on the ionization chamber and a LaBr gate on the $9/2^+ \rightarrow (3/2, 5/2)^+$ (308.3 keV) transition. (c) The interpolated background time response with the reference energy of 355.4 keV for the feeding transition of the $(3/2, 5/2)^+$ state. (d) The interpolated background time response with the reference energy of 308.3 keV for the decaying transition of the $(3/2, 5/2)^+$ state. (e) The resulting time distribution for the $(3/2, 5/2)^+$ state at 522.5 keV. (f) and (g) The 141.0 (167.1)-keV transition after applying an ionization chamber gate in $A = 97$ and a LaBr gate in the $3/2^+ \rightarrow 1/2^+$ ($7/2^+ \rightarrow 3/2^+$) transition with an energy of 167.1 (141.0) keV. (h) The resulting time distribution for the $3/2^+$ state at 167.1 keV, where three different methods were used to determine the lifetime.

To describe ^{97}Sr an IBFM Hamiltonian, $\hat{H}_{\rm IBFM}$, is used which is the sum of the neutron-proton IBM (IBM-2) Hamiltonian $\hat{H}_{\rm B}$, the single-particle fermion Hamiltonian $\hat{H}_{\rm F}$, and the boson-fermion interaction term $\hat{H}_{\rm BF}$:

$$\hat{H}_{\rm IBFM} = \hat{H}_{\rm B} + \hat{H}_{\rm F} + \hat{H}_{\rm BF}. \quad (6)$$

In the IBM-2 model, pairs of protons (neutrons) are coupled to spin $J = 0^+$ s_π (s_ν) bosons and to $J = 2^+$ d_π (d_ν) bosons, respectively [45]. For ^{97}Sr which has ten valence protons and nine valence neutrons out of the ^{78}Ni doubly magic core, five proton bosons and four neutron bosons are used for the IBM-2 Hamiltonian $\hat{H}_{\rm B}$ part of Eq. (6). The determination of the parameters of the IBM-2 Hamiltonian $\hat{H}_{\rm B}$ is described in Ref. [41]. It relies on the (β, γ)-deformation energy surfaces computed using a constrained HFB method [46] which is based on the parametrization D1M of the Gogny EDF [41,47,48]. To describe the neutron that remains after coupling the neutron/proton bosons, the fermion valence space was chosen to be the $3s_{1/2}$, $2d_{3/2}$, $2d_{5/2}$ and $1g_{7/2}$ orbitals of the whole neutron major shell $N = 50$–82 [41]. The last part of the IBFM Hamiltonian, which is the boson-fermion interaction part $\hat{H}_{\rm BF}$, is taken from Ref. [41]:

$$\hat{H}_{\rm BF} = \Gamma_\nu \hat{Q}^{(2)}_\pi \cdot \hat{q}^{(2)}_\nu + \Lambda_\nu \hat{V}_{\pi\nu} + A_\nu \hat{n}_{d\nu} \hat{n}_\nu. \quad (7)$$

The product of the strength constant Γ_ν times the boson quadrupole operator for proton bosons $\hat{Q}^{(2)}_\pi$ times the quadrupole operator for the odd neutron $\hat{q}^{(2)}_\nu$ represents the quadrupole dynamical term [41]. The second term describes the exchange interaction introduced to consider that the bosons are in fact nucleon pairs. Both the quadrupole dynamical and the exchange terms act predominantly between protons and neutrons [41]. The last part is the monopole interaction, which is the product of the strength A_ν and the number operator for neutron d bosons, and neutron fermion $\hat{tn}_\nu$ acts between like particles (i.e., between odd neutrons and neutron bosons) [41].

For the calculations of ^{97}Sr, the even-even core ^{96}Sr has been used, which shows a weakly oblate-deformed ground-state minimum and in which the IBFM-2 Hamiltonian is built. The used energy potential surface is shown in Fig. 2 of Ref. [44], which has a pronounced prolate ground-state minimum [44].

B. Energy levels

The results from the IBFM calculations and the experimental energy levels are visualized in Fig. 4. The first two states of the calculation, i.e., the $1/2^+$ and $3/2^+$ states, are in good agreement with the experimental energies. The experimental energy of the $7/2^+_1$ state cannot be properly described by the calculation. The calculation cannot clearly classify the spin of the $(3/2, 5/2)^+$ state at 522 keV using only energetic arguments. On the one hand the first calculated $5/2^+$ state is approximately in the energy region of the $(3/2, 5/2)^+$ state, but it is lower than the state of interest. On the other hand the calculated $3/2^+$ state could be assigned to the state of interest, but as Fig. 2 shows, two other $3/2^+$ states are located nearby this state, i.e., at 585 and 600 keV. This makes it difficult to draw a conclusion about the spin of the level at

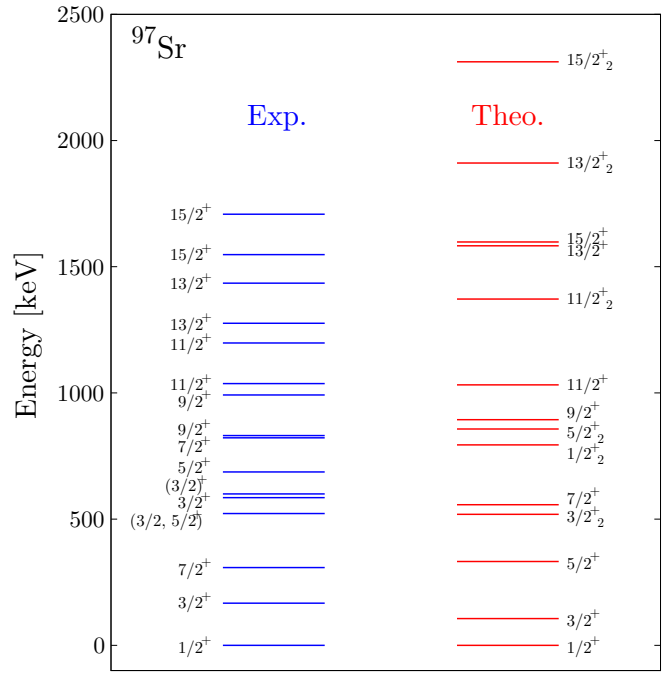

FIG. 4. The experimental (left) and theoretical (right) states with their spins and energies for ^{97}Sr up to 2.5 MeV. The experimental energies and spins are taken from Refs. [14,49–51].

522 keV from energy consideration, but further arguments about the state are given in the second part of the discussion, where the $B(E2)$ value is involved to classify the state. The experimentally observed energy of the $9/2^+$ state can be described by the model. Note that the calculated $9/2^+$ state lies in between the experimental $9/2^+_1$ and $9/2^+_2$ states, but closer to the $9/2^+_1$ state in this work. For higher states, which were not observed in this work, only the $11/2^+$ state is in good agreement with the experimental energy. The other states are mostly calculated to be higher than the experimental ones.

Furthermore, the percentage composition values of the IBFM wave function for the neutron single-particle orbitals, i.e., for the $3s_{1/2}$, $2d_{3/2}$, $2d_{5/2}$, and $1g_{7/2}$ orbitals, are given in Table I. The compositions of the $1/2^+_1$ state and the $5/2^+_1$ state have a large overlap, which may lead to the assumption that the supposed $5/2^+_1$ state could be spherical as the ground state. Additionally, the overlap of the compositions of the $3/2^+_1$ and $7/2^+_1$ states is also very large. The higher-lying $9/2^+$ state consists mainly of the $2d_{3/2}$ orbital and the $2d_{5/2}$ orbital, where a description with the highly deformed intruder $\nu 9/2$ [404] Nilsson orbital could be a better description [14,36,38]. The intruder $\nu 9/2$ [404] Nilsson orbital has also been observed in the corresponding isotone ^{99}Zr [52], but not for ^{101}Mo and ^{95}Kr, which could be due to the special proton-neutron configuration in the Sr and Zr isotopes.

C. Transition probabilities

In Table II all lifetimes and corresponding reduced transition strengths are summarized. Due to the lack of knowledge about the spin of the state at 522 keV, which could be a $3/2^+$ state or a $5/2^+$ state [6], the transitions which decay or feed

TABLE I. The composition of the IBFM wave function for the neutron single-particle orbitals ($3s_{1/2}$, $2d_{3/2}$, $2d_{5/2}$, $1g_{7/2}$) for ^{97}Sr. The values are all given in percentages and only for positive-parity states.

	^{97}Sr			
J	$3s_{1/2}$	$2d_{3/2}$	$2d_{5/2}$	$1g_{7/2}$
$1/2^+_1$	12	24	56	8
$3/2^+_1$	10	20	65	5
$5/2^+_1$	12	25	54	9
$3/2^+_2$	16	41	21	22
$7/2^+_1$	10	22	61	7
$1/2^+_2$	16	36	31	17
$5/2^+_2$	14	46	17	23
$9/2^+_1$	11	32	43	14
$11/2^+_1$	17	46	9	28
$11/2^+_2$	11	22	58	9
$13/2^+_1$	10	38	33	19
$15/2^+_1$	16	51	3	30
$13/2^+_2$	13	25	48	14
$15/2^+_2$	10	35	35	20

this state have unknown multipolarities. For the other states, i.e., $1/2^+$, $3/2^+$, $7/2^+$, and $9/2^+$, the spins were know, but not all the multipolarities of the transitions connecting them were known. Therefore, the reduced transition strength for some of the states is given in an $E2$ or a $M1$ limit, where we assume that the transition is either a pure $E2$ or a pure $M1$ character.

The $7/2^+ \rightarrow 3/2^+$ and $3/2^+ \rightarrow 1/2^+$ transitions were found to be pure $E2$ and pure M1 transitions, respectively [33]. The calculated $B(M1)$ value for the $3/2^+ \rightarrow 1/2^+$ transition is a factor of 2 higher than the experimental value. Also, the $B(E2)$ for the $7/2^+ \rightarrow 3/2^+$ transition is calculated an order of magnitude too high. The large discrepancy for both states could reflect the similarity between both states (see Table II), which could arise from the employed single-particle energies, the occupation probabilities, and the fitted strength parameters for the boson-fermion interactions.

The $9/2^+$ state decays via an $E2$ transition to the $5/2^+$ state at 522 keV and via a mixed $M1/E2$ transition to the $7/2^+$ state at 167 keV. A $5/2^+$ state is preferred, because a $3/2^+$ spin would suggest an $M3/E4$ transition which seems very unlikely. Further reasons for the preference of a $5/2^+$ spin are given in the next section. The calculated $B(M1)$ and $B(E2)$ strength values overestimate the experimental values in all cases.

D. The (3/2, 5/2)$^+$ state at 522 keV

The state at 522 keV is a bit more complicated to describe, because the spin of the state is either $3/2^+$ or $5/2^+$ [6]. For two of the three decaying transitions of the state, i.e., 522.5 keV ($3/2^+$, $5/2^+ \rightarrow 1/2^+$) and 214.4 keV ($3/2^+$, $5/2^+ \rightarrow 7/2^+$) the transitions could be of $E2$ or $M1$ character depending on whether the initial state is $3/2^+$ or $5/2^+$. Only the 355.4-keV ($3/2^+$, $5/2^+ \rightarrow 3/2^+$) transition has a known multipolarity, which is $M1$ [6]. Let us first assume the state has spin and parity $3/2^+$, so that the state is $3/2^+_2$. Then the $3/2^+_2 \rightarrow 1/2^+$ transitions could be an $M1$, an $E2$, or a

TABLE II. The investigated and observed states of ^{97}Sr, where the energy of the initial and final levels, the lifetime, the transitions with their multipolarity, the reduced transition probability $B(E2)$, and $B(M1)$ are given. In cases where experimental multipole mixing ratios are missing or the type and the multipolarity of the transition are unclear, the transition probabilities are calculated by assuming the limits of a pure $E2$ or $M1$ transition, which are marked with *. Further details about different transitions are given in the text.

				Experimental results from this work		Theory
E_{Level} (keV)	$J^{\pi 2} \rightarrow J^{\pi 1}$	Intensity[a]	Multipolarity	$\tau(J^{\pi 2})$	$B(\sigma\lambda; J^{\pi 2} \rightarrow J^{\pi 1})$	$B(\sigma\lambda)$
167.1	$3/2^+ \rightarrow 1/2^+$	100	$M1$	448(4) ps	$260(2)\times10^{-4}\ \mu_N^2$	$52 \times 10^{-3}\ \mu_N^2$
308.1	$7/2^+ \rightarrow 3/2^+$	100	$E2$	252(10) ns	$45(2)\ e^2\ \text{fm}^4$	$740\ e^2\ \text{fm}^4$
522.5[b]	$5/2^+ \rightarrow 1/2^+$	4(1)	$E2$	14(6) ps	$450^{+330}_{-140}\ e^2\ \text{fm}^4$	$313\ e^2\ \text{fm}^4$
	$\rightarrow 3/2^+$	100(8)	$M1$		$60^{+40}_{-20} \times 10^{-3}\ \mu_N^2$	$120 \times 10^{-3}\ \mu_N^2$
	$\rightarrow 7/2^+$	46(6)	$E2$*		$3300^{+2700}_{-1300}\ e^2\ \text{fm}^4$	$128\ e^2\ \text{fm}^4$
			$M1$*		$11^{+9}_{-4} \times 10^{-3}\ \mu_N^2$	$96 \times 10^{-3}\ \mu_N^2$
522.5[c]	$3/2^+_2 \rightarrow 1/2^+$	4(1)	$E2$*	14(6) ps	$450^{+330}_{-140}\ e^2\ \text{fm}^4$	$33\ e^2\ \text{fm}^4$
			$M1$*		$9^{+6}_{-3} \times 10^{-3}\ \mu_N^2$	$29 \times 10^{-3}\ \mu_N^2$
	$\rightarrow 3/2^+$	100(8)	$M1$		$60^{+40}_{-20} \times 10^{-3}\ \mu_N^2$	$17 \times 10^{-3}\ \mu_N^2$
	$\rightarrow 7/2^+$	46(6)	$E2$		$3300^{+2700}_{-1300}\ e^2\ \text{fm}^4$	$4\ e^2\ \text{fm}^4$
830.8	$9/2^+ \rightarrow 5/2^+$[d]	3.2(12)	$E2$	759(25) ns	$12^{+7}_{-5} \times 10^{-3}\ e^2\ \text{fm}^4$	$398\ e^2\ \text{fm}^4$
	$\rightarrow 7/2^+$	100(28)	$E2$*		$27(1)\times10^{-3}\ e^2\ \text{fm}^4$	$31\ e^2\ \text{fm}^4$
			$M1$*		$51(2)\times10^{-8}\ \mu_N^2$	$102 \times 10^{-3}\ \mu_N^2$

[a]The intensities are taken from Refs. [31,49].
[b]By assuming it is a $5/2^+$ state.
[c]By assuming it is a $3/2^+$ state.
[d]A $5/2^+$ state is preferred, because a $3/2^+$ would suggest am $M3/E4$ transition that is unlikely.

mixed $M1/E2$ transition. The multipolarity and the multipole mixing ratio are unknown and therefore the extreme limits of an $M1$ transition and an $E2$ transition are given and compared to the IBFM calculations (see Table II). The calculation underestimates the $B(E2)$ strength and overestimates the $B(M1)$ strength, by which one could conclude that the transition contains both multipolarities. The second transition, i.e., $3/2^+ \rightarrow 7/2^+$, would correspond to an $E2$ transition. The experimentally determined $B(E2)$ value is 3 orders of magnitude higher than the calculated $B(E2)$ value. Note that the experimental value has high uncertainties, which results from the high uncertainty of the lifetime but also from the imprecisely measured branching ratio with 3(1) [31]. For the $3/2_2^+ \rightarrow 3/2_1^+$ transition the multipolarity of $M1$ has been determined [6]. The calculated $B(M1)$ strength underestimates the experimental value by a factor of 3, which is therefore the least discrepant described transition probability by the model. Now the values are discussed within the assumption that the state has spin and parity of $5/2^+$. The $5/2^+ \rightarrow 1/2^+$ transition is a pure $E2$ transition, where the experimental $B(E2)$ value of 451^{+329}_{-142} e^2 fm^4 is described by the calculated value of 313 e^2 fm^4. The second transition, i.e., $5/2^+ \rightarrow 7/2^+$, has a mixed $M1/E2$ character in which the experimental $B(M1)$ value, which is calculated by assuming a pure $M1$ transition, is overestimated by the calculation. The opposite case occurs for the experimental $B(E2)$ value, where a pure $E2$ transition is assumed, in which the calculation underestimates the value by an order of magnitude. For the known $M1$ transition $5/2^+ \rightarrow 3/2^+$, the calculation is twice as big as the experimental $B(M1)$ value, which is quite accurate in contrast to the other transition strengths.

With the newly measured results and the theoretical calculations the spin of the state at 522 keV is discussed in the following. First, the calculated $3/2_2^+$ state is very close in energy to the state at 522 keV, but this state could also be assigned to the experimental $3/2^+$ state at 585 or 600 keV. Furthermore, by looking at the calculated $3/2_1^+$ state compared to the experimental $3/2_1^+$ state it seems likely that the calculation is underestimating the energy of the states in this region. This could lead to the conclusion that the calculated $5/2^+$ state is also underestimated. Hence, a higher energy is expected that would fit better to the state at 522 keV. Another fact is that the calculated transition strength by assuming a $5/2^+$ state describes the experimental values better. According to Ref. [31], where a partial half-life of 16.6(3) μs is obtained for the 308.3-keV transition from the $9/2^+$ state, an $E2$ transition is favored because an $M3$ multipolarity would be incompatible with the partial half-life [31]. Additionally, earlier observed experimental signatures recommend a $5/2^+$ state like the enhanced transition rate of the $(3/2, 5/2)^+$ state at 600.5 keV, which can be described as being the $1/2^+_{\text{g.s.}} \otimes 2^+_{\text{phonon}}$ first quadrupole vibrational state [5]. The experimental data of ^{97}Sr seem to show no other remaining possibility to create a $5/2^+$ state at 522 keV with a collective nature, and therefore it is likely to be a high-seniority, spherical shell-model state [31]. Note that the $3/2_1^+$ state has been described as a high-seniority, spherical shell-model state [6], where the state is weakly fed via the β decay of the deformed nucleus ^{97}Rb [6,31]. The β decay between those state occurs with a high log $ft = 6.5$ value, which is a first forbidden transition type and could be a hint of shape hindrance in this transition [6,31]. Nearly the same log ft value has been reported for the state at 522 keV [6], which is an indication of a similar structure for this level [31]. According to the number of supporting experimental facts and the additional support from the IBFM calculation we suggest a spin assignment of $5/2^+$ for the state at 522 keV, although a structure corresponding to a high-seniority spherical shell-model state is also possible.

VI. CONCLUSIONS

The lifetimes of all the states that are fed by the isomeric $9/2^+$ state and the lifetime of the isomeric state itself could be measured. The lifetime of the $7/2^+$ and $9/2^+$ isomers could be confirmed within the results of some earlier works. The experimental results of the $3/2^+$ state do not agree with the literature values, where we prefer the result from this work due to the high statistics and improved technique. An important observed state was the $(3/2, 5/2)^+$ state at 522 keV, where the lifetime and the resulting transition strength lead to the suggestion that the state is a $5/2^+$ state and likely to be a high-seniority shell-model state. Based on the new experimental data of ^{97}Sr, which is exactly at the spherical-deformed border, the nuclear structure of the $5/2^+$ state gives a hint, where the deformed configuration of the nucleus is preferred. Further experiments to determine the multipolarities of the transitions would be desirable.

ACKNOWLEDGMENTS

We thank the team of the nuclear reactor for the operation at the ILL. A.E. and V.K. acknowledge the financial support by the BMBF under Grant No. 05P15PKFNA. J.-M.R. and L.K. acknowledge the financial support by the Deutsche Forschungsgemeinschaft (DFG) under Grant No. JO391/16-2. The work of the author K.N. is financed within the Tenure Track Pilot Programme of the Croatian Science Foundation and the École Polytechnique Fédérale de Lausanne and Project No. TTP-2018-07-3554, Exotic Nuclear Structure and Dynamics, with funds of the Croatian-Swiss Research Programme. The work of L.M.R. was partly supported by the Spanish MINECO under Grants No. FPA2015-65929 and No. FIS2015-63770. The open access fee was covered by FILL2030, a European Union project within the European Commission's Horizon 2020 Research and Innovation programme under Grant Agreement No. 731096.

[1] E. Clément *et al.*, Phys. Rev. Lett. **116**, 022701 (2016).
[2] J.-M. Régis *et al.*, Phys. Rev. C **95**, 054319 (2017).
[3] S. Brant, G. Lhersonneau, and K. Sistemich, Phys. Rev. C **69**, 034327 (2004).

[4] K. Kawade, G. Battistuzzi, H. Lawin, H. A. Selič, K. Sistemich, F. Schussler, E. Monnand, J. A. Pinston, B. Pfeiffer, and G. Jung, Z. Phys. A: At. Nucl. **304**, 293 (1982).

[5] M. Büscher, R. F. Casten, R. L. Gill, R. Schuhmann, J. A. Winger, H. Mach, M. Moszyński, and K. Sistemich, Phys. Rev. C **41**, 1115 (1990).

[6] G. Lhersonneau, B. Pfeiffer, K. L. Kratz, H. Ohm, K. Sistemich, S. Brant, and V. Paar, Z. Phys. A: At. Nucl. **337**, 149 (1990).

[7] P. Spagnoletti *et al.*, Phys. Rev. C **100**, 014311 (2019).

[8] H. Mach, M. Moszyński, R. Gill, F. Wohn, J. Winger, J. C. Hill, G. Molnár, and K. Sistemich, Phys. Lett. B **230**, 21 (1989).

[9] F. Schussler, J. Pinston, E. Monnand, A. Moussa, G. Jung, E. Koglin, B. Pfeiffer, R. Janssens, and J. van Klinken, Nucl. Phys. A **339**, 415 (1980).

[10] K. Becker, G. Jung, K. H. Kobras, H. Wollnik, and B. Pfeiffer, Z. Phys. A: At. Nucl. **319**, 193 (1984).

[11] J. Skalski, S. Mizutori, and W. Nazarewicz, Nucl. Phys. A **617**, 282 (1997).

[12] R. Rodríguez-Guzmán, P. Sarriguren, L. Robledo, and S. Perez-Martin, Phys. Lett. B **691**, 202 (2010).

[13] R. A. Meyer, Hyperfine Interact. **22**, 385 (1985).

[14] W. Urban, J. A. Pinston, J. Genevey, T. Rząca-Urban, A. Złomaniec, G. Simpson, J. L. Durell, W. R. Phillips, A. G. Smith, B. J. Varley, I. Ahmad, and N. Schulz, Eur. Phys. J. A **22**, 241 (2004).

[15] P. Federman and S. Pittel, Phys. Lett. B **69**, 385 (1977).

[16] P. Federman and S. Pittel, Phys. Lett. B **77**, 29 (1978).

[17] P. Federman and S. Pittel, Phys. Rev. C **20**, 820 (1979).

[18] M. Albers *et al.*, Phys. Rev. Lett. **108**, 062701 (2012).

[19] P. Armbruster, M. Asghar, J. Bocquet, R. Decker, H. Ewald, J. Greif, E. Moll, B. Pfeiffer, H. Schrader, F. Schussler, G. Siegert, and H. Wollnik, Nucl. Instrum. Methods **139**, 213 (1976).

[20] G. Fioni, H. Faust, M. Gross, M. Hesse, P. Armbruster, F. Gönnenwein, and G. Münzenberg, Nucl. Instrum. Methods Phys. Res., Sect. A **332**, 175 (1993).

[21] J.-M. Régis, A. Esmaylzadeh, G. Häfner, J. Jolie, V. Karayonchev, Y. H. Kim, L. Knafla, U. Köster, C. Michelagnoli, M. Rudigier, and G. Simpson, Study of the abrupt shape changes in 97Sr (Institut Laue-Langevin, 2018), doi: 10.5291/ILL-DATA.3-01-659.

[22] U. Köster, H. Faust, T. Materna, and L. Mathieu, Nucl. Instrum. Methods Phys. Res., Sect. A **613**, 363 (2010).

[23] J.-M. Régis *et al.*, Nucl. Instrum. Methods Phys. Res., Sect. A (to be published).

[24] J.-M. Régis, N. Saed-Samii, M. Rudigier, S. Ansari, M. Dannhoff, A. Esmaylzadeh, C. Fransen, R.-B. Gerst, J. Jolie, V. Karayonchev, C. Müller-Gatermann, and S. Stegemann, Nucl. Instrum. Methods Phys. Res., Sect. A **823**, 72 (2016).

[25] J.-M. Régis, M. Dannhoff, and J. Jolie, Nuclear Instrum. Methods Phys. Res., Sect. A **897**, 38 (2018).

[26] J.-M. Régis *et al.*, Nucl. Instrum. Methods Phys. Res., Sect. A **726**, 191 (2013).

[27] Z. Bay, Phys. Rev. **77**, 419 (1950).

[28] S. Ansari *et al.*, Phys. Rev. C **96**, 054323 (2017).

[29] A. Esmaylzadeh, L. M. Gerhard, V. Karayonchev, J.-M. Régis, J. Jolie, M. Bast, A. Blazhev, T. Braunroth, M. Dannhoff, F. Dunkel, C. Fransen, G. Häfner, L. Knafla, M. Ley, C. Müller-Gatermann, K. Schomacker, N. Warr, and K.-O. Zell, Phys. Rev. C **98**, 014313 (2018).

[30] V. Karayonchev, A. Blazhev, A. Esmaylzadeh, J. Jolie, M. Dannhoff, F. Diel, F. Dunkel, C. Fransen, L. M. Gerhard, R.-B. Gerst, L. Knafla, L. Kornwebel, C. Müller-Gatermann, J.-M. Régis, N. Warr, K. O. Zell, M. Stoyanova, and P. Van Isacker, Phys. Rev. C **99**, 024326 (2019).

[31] M. Rudigier, G. S. Simpson, J. M. Daugas, A. Blazhev, C. Fransen, G. Gey, M. Hackstein, J. Jolie, U. Köster, T. Malkiewicz, T. Materna, M. Pfeiffer, M. Ramdhane, J.-M. Régis, W. Rother, T. Thomas, N. Warr, D. Wilmsen, J. Le Bloas, and N. Pillet, Phys. Rev. C **87**, 064317 (2013).

[32] H. Ohm, G. Lhersonneau, K. Sistemich, B. Pfeiffer, and K. L. Kratz, Z. Phys. A **327**, 483 (1987).

[33] K. L. Kratz, H. Ohm, A. Schröder, H. Gabelmann, W. Ziegert, B. Pfeiffer, G. Jung, E. Monnand, J. A. Pinston, F. Schussler, G. I. Crawford, S. G. Prussin, and Z. M. de Oliveira, Z. Phys. A **312**, 43 (1983).

[34] M. Czerwiński, T. Rzaca-Urban, W. Urban, P. Baczyk, K. Sieja, B. M. Nyakó, J. Timár, I. Kuti, T. G. Tornyi, L. Atanasova, A. Blanc, M. Jentschel, P. Mutti, U. Köster, T. Soldner, G. de France, G. S. Simpson, and C. A. Ur, Phys. Rev. C **92**, 014328 (2015).

[35] J. K. Hwang, A. V. Ramayya, J. H. Hamilton, Y. X. Luo, A. V. Daniel, G. M. Ter-Akopian, J. D. Cole, and S. J. Zhu, Phys. Rev. C **73**, 044316 (2006).

[36] J. K. Hwang *et al.*, Phys. Rev. C **67**, 054304 (2003).

[37] R. E. Sund, H. Weber, and V. V. Verbinski, Phys. Rev. C **10**, 853 (1974).

[38] A. Złomaniec, H. Faust, J. Genevey, J. A. Pinston, T. Rząca-Urban, G. S. Simpson, I. Tsekhanovich, and W. Urban, Phys. Rev. C **72**, 067302 (2005).

[39] D. Kameda *et al.*, Phys. Rev. C **86**, 054319 (2012).

[40] F. Iachello and P. v. Isacker, *The Interacting Boson-Fermion Model*, Cambridge Monographs on Mathematical Physics (Cambridge University, Cambridge, England, 1991).

[41] K. Nomura, R. Rodríguez-Guzmán, and L. M. Robledo, Phys. Rev. C **97**, 064313 (2018).

[42] K. Nomura, T. Nikšić, and D. Vretenar, Phys. Rev. C **93**, 054305 (2016).

[43] K. Nomura, R. Rodríguez-Guzmán, and L. M. Robledo, Phys. Rev. C **96**, 014314 (2017).

[44] K. Nomura, R. Rodríguez-Guzmán, and L. M. Robledo, Phys. Rev. C **94**, 044314 (2016).

[45] T. Otsuka, A. Arima, and F. Iachello, Nucl. Phys. A **309**, 1 (1978).

[46] R. Rodríguez-Guzmán, P. Sarriguren, L. M. Robledo, and J. E. García-Ramos, Phys. Rev. C **81**, 024310 (2010).

[47] J. Decharge, M. Girod, and D. Gogny, Phys. Lett. B **55**, 361 (1975).

[48] S. Goriely, S. Hilaire, M. Girod, and S. Péru, Phys. Rev. Lett. **102**, 242501 (2009).

[49] National Nuclear Data Center (NNDC), Nuclear Levels and Gamma Search, 05/2018.

[50] W. Urban, J. Durell, A. Smith, W. Phillips, M. Jones, B. Varley, T. Rząca-Urban, I. Ahmad, L. Morss, M. Bentaleb, and N. Schulz, Nucl. Phys. A **689**, 605 (2001).

[51] C. Y. Wu, H. Hua, D. Cline, A. B. Hayes, R. Teng, R. M. Clark, P. Fallon, A. Goergen, A. O. Macchiavelli, and K. Vetter, Phys. Rev. C **70**, 064312 (2004).

[52] W. Urban, J. Pinston, T. Rzaca-Urban, A. Złomaniec, G. Simpson, J. Durell, W. Phillips, A. Smith, B. Varley, I. Ahmad, and N. Schulz, Eur. Phys. J. A **16**, 11 (2003).